Real-Time Characterization of Phosphate Powder With Microwave Sensor: Investigating the Impact of Temperature

Youness Zaarour, *Student Member, IEEE*, Fatima Zahrae El Arroud, *Student Member, IEEE*, Otman El Mrabet, *Member, IEEE*, Abdessamad Faik, Rafiq El Alami, and Hafid Griguer, *Member, IEEE*

***Abstract*—Temperature control in the industrial use of phosphate ensures chemical stability, which affects product quality and process efficiency. This study introduces a novel approach employing a microwave sensor with a double-hexagonal complementary split-ring resonator (DH-CSSR) for real-time control and monitoring of industrial phosphate powders, focusing on temperature-induced variations. Operating within the 0.1–4-GHz frequency range, the sensor detects shifts in the resonance frequency of the S-parameters, which are indicative of alterations in the dielectric properties of the phosphate powder as a function of temperature variations. A comparative evaluation with simulated outcomes, incorporating permittivity values ascertained through a coaxial probe at diverse temperatures, establishes a robust congruence between experimental and simulated datasets. Root mean square error (RMSE) values of 0.44, 2.2, and 3.28 for the first, second, and third resonances, respectively, underscore the sensor's precision in mirroring the actual conditions of phosphate powder encountered during storage and transportation. Such accuracy underscores the sensor's potential in accurately representing real-world conditions of phosphate powder, thus facilitating the optimization of crop yield through enhanced management of phosphate powder characteristics.**

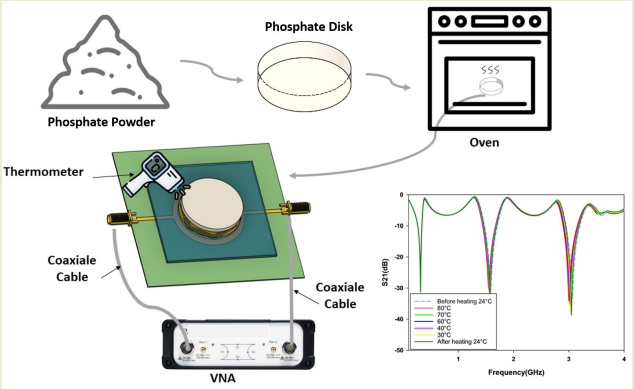

***Index Terms*— Dielectric properties, microwave sensor, phosphate powder, storage, transportation.**

I. Introduction

With continuous expansion in global industries, the demand for superior phosphate is intensifying, underlining their indispensable role in various manufacturing processes. Phosphate, essential for a range of industrial applications from detergents to food additives and water treatment, is central to the efficiency and sustainability of these industries. Given the diverse applications of phosphate, ensuring its purity and quality is paramount, not only for the operational success of industries but also for environmental conservation and public health [1], [2]. The global phosphate market, valued at approximately 68 billion dollars in 2021, is projected to grow significantly due to increasing demands in the agriculture, food processing, and water treatment sectors. However, this growth is coupled with challenges, including the sustainable and responsible sourcing of phosphate, minimizing environmental impact, and adhering to stringent regulatory standards. For instance, the industrial sector's reliance on phosphate necessitates rigorous quality control measures to prevent contamination that could lead to significant ecological and health issues, such as eutrophication of water bodies and adverse health effects from contaminated products [3], [4].

Real-time monitoring of phosphate quality is crucial in industrial settings, where the precision of phosphate composition directly influences process efficiency, product durability, and environmental compliance. Industries such as metal treatment, ceramics, and electronics depend on the consistent quality of phosphate for optimal results. Variations in phosphate quality due to improper handling, storage,

Manuscript received 13 June 2024; accepted 15 July 2024. Date of publication 24 July 2024; date of current version 1 September 2024. This work was supported by the Ph.D. Student Grant of the University of Mohammed VI Polytechnique (UM6P). The associate editor coordinating the review of this article and approving it for publication was Prof. Yuedong Xie. *(Corresponding author: Youness Zaarour.)*

Youness Zaarour, Fatima Zahrae El Arroud, Rafiq El Alami, and Hafid Griguer are with Microwave Energy Sensing (MES), DICE—Digital Innovation Center of Excellence, University of Mohammed VI Polytechnic, Ben Guerir 43152, Morocco (e-mail: youness.zaarour@um6p.ma).

Otman El Mrabet is with the System of Information and Telecommunications Laboratory (LaSIT), FS, Abdelmalek Essaadi University, Tetouan 93000, Morocco.

Abdessamad Faik is with the Laboratory for Inorganic Materials for Sustainable Energy Technologies (LIMSET), University of Mohammed VI Polytechnic, Ben Guerir 43152, Morocco.

Digital Object Identifier 10.1109/JSEN.2024.3430490

or chemical changes can affect the effectiveness of processes such as metal coatings and ceramic manufacturing, leading to increased waste, rework, and potential environmental hazards. Implementing advanced real-time monitoring systems enables industries to make immediate adjustments, ensuring consistent product quality, reducing ecological impact, and adhering to strict environmental regulations, thus underscoring the importance of such technologies in modern industrial practices [5], [6].

The quality control of soil and phosphate powder often relies on advanced analytical techniques such as near-infrared spectroscopy (NIR), chromatography, and X-ray fluorescence (XRF) analysis due to their high precision and accuracy. NIR spectroscopy is based on measuring the amount of light absorbed and reflected by an analyzed substance or material across a broad range of wavelengths (typically between 800 and 2500 nm) that enable it to obtain its chemical composition. Chromatography, on the other hand, separates complex mixtures into their individual components. In contrast, XRF analysis is a rapid approach to determining the elemental composition of materials such as soil. This technique does not require any preanalysis acid digestion techniques that are typically used in laboratory procedures, making it a valuable screening tool for soil analysis. It can provide an accurate and complete analysis of the elemental composition of a sample, making it useful for monitoring soil and phosphate powder quality and identifying any potential contaminants. However, these methods offer effective means for controlling soil and phosphate quality, demanding skilled personnel, advanced laboratory infrastructure, intricate solution preparation, costly equipment, and the utilization of carcinogenic substances. Hence, it is crucial to develop new techniques that are affordable, offer rapid measurement capabilities, and utilize portable instruments for monitoring and managing phosphate quality [7], [8], [9].

Microwave sensor application offers a viable alternative to address the shortcomings of conventional analytical methodologies. Zhu and Huang [10] offer an extensive analysis of coaxial cable sensing methods, emphasizing their uses in nondestructive, real-time testing and measuring settings. By utilizing the special interactions that exist between microwaves and materials, this technique evaluates dielectric properties, which are connected with the chemical composition and quality metrics of the materials. Similarly, Jonathan Muñoz-Enano et al. [11] investigate the advancement and possibilities of planar microwave resonant sensors, emphasizing their accuracy and potential integration into portable electronics. These sensors offer several advantages, including rapid measurement times, reduced need for sample preparation, and the potential for on-site analysis without the necessity for extensive safety measures or highly skilled operators, expanding the utility of microwave sensors beyond mere industrial applications [12], [13]. These technologies have proven to be invaluable across a spectrum of fields, demonstrating significant outcomes in the medical sector by identifying tumors [14], [15], ensuring the quality and temperature control of pharmaceuticals [16], and monitoring glucose levels [17], [18]. Moreover, RF and microwave sensors have been utilized in chemical [19], [20] and biological processes [21], showcasing their adaptability and versatility. Specifically, they have been used for real-time measurement in humidity sensing [22], detecting moisture and Fe particles in oil [23], and monitoring swelling phenomena caused by a dynamic range of target gas molecules [24].

With such diverse applications, including agricultural monitoring and information provision, these sensors are well-suited for characterizing and monitoring the quality of phosphate powder. Microwave sensors have demonstrated the potential to monitor nitrate and phosphate concentration [25], [26]. It is worth mentioning that changes in temperature can affect the dielectric properties of phosphate powder [15].

The novelty of this work lies in our unique approach to analyzing the effects of temperature on phosphate samples. Specifically, we focus on the permanent changes in the phosphate's properties induced by heating. To the best of our knowledge, up until now, there is no published paper in the literature that explores this issue. The study utilizes a microwave sensor as a key tool to assess the properties of phosphate powder while subjecting it to varying temperature conditions. The article is organized as follows. Section I outlines the configuration of the proposed filter-based sensor and measurement of the permittivity (both real and imaginary parts) of the phosphate powder at varying temperature values by using the coaxial probe technique. Subsequently, these measured data representing the phosphate powder permittivity were implemented into the simulation software. This step helps us to perform numerical simulations using a high-frequency structure simulator (HFSS) and explore the effect of the temperature on the phosphate powder. The experimental results of the sensor are then elucidated and discussed in Section III. Finally, Section IV presents preliminary conclusions.

II. Materials and Methods

A. Sensor Design and Methodology

A small-sized microwave filter-based sensor has been developed to examine temperature-induced changes in phosphate powder, mainly by evaluating permittivity fluctuations. The core detecting area of the sensor is a circular patch containing double-hexagonal complementary split-ring resonators (DH-CSRRs). The hexagonal shape was selected to benefit from the longer sides, which boosts electromagnetic field interaction and improves sensitivity. Moreover, the hexagonal arrangement offers an advantage over the circular form by concentrating the field lines in a smaller region, enhancing the interaction between the sensor and the material under test (MUT). The patch is placed between two 50-Ω transmission lines with a width of 2.44 mm and printed on a Rogers 5880 substrate, which has a dielectric permittivity of 2.2, a loss tangent of 0.0009, and a thickness of 0.787 mm. The overall dimensions of the structure are 100×100 mm^2. The detailed parameters of the DH-CSRR are provided in millimeters and are presented in Fig. 1(a). A plexiglass holder with dimensions of 30×30 mm and a thickness of 3 mm is used to position the sample. The holder has a cavity that secures the sample in direct contact with the top of the sensor over the sensing area, as shown in Fig. 1(b). The sensor and its plexiglass holder

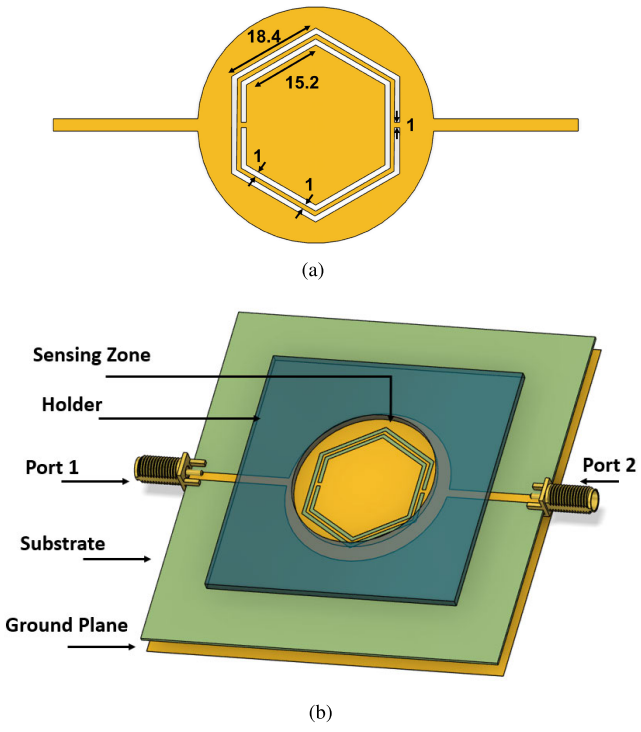

Fig. 1. (a) Top view of the sensor with hexagonal CSRR geometry and dimensions in millimeters. (b) 3-D view of the sensor setup, showing the holder, substrate, ground plane, and ports (Ports 1 and 2), with the sensing zone highlighted.

are fabricated using a high-quality computer numerical control (CNC) milling process. This design facilitates the convenient placement of the phosphate sample in the sensing zone, which is crucial for effective interaction between the sample and the electric fields, leading to accurate readings and improved sensitivity in measuring the sample's dielectric properties.

Up until now, the complementary split-ring resonator (CSRR) remains the main element for developing numerous metamaterial microwave circuits owing to its subwavelength dimensions at the quasistatic resonant frequency. This feature helps to design compact microwave devices such as antennas, filters, and sensors [27]. The SRR resonator is generally placed on the upper side of the sensor sandwiched between two microstrip lines. The CSRR is excited by the current in the microstrip line that can flow in the outer ring. A magnetic field can then be induced by the excitation of the displacement currents in the CSRR and, hence, the apparition of a magnetic resonance. It is important to note that CSRR is widely known for its simultaneous magnetoelectric response [28]. When a MUT is placed directly over or in close proximity to the complementary split-ring resonator (CSRR), it induces a disturbance in the electromagnetic field distribution surrounding the resonator, leading to a variation in the resonant frequency. This perturbation in electromagnetic energy is intricately linked to the dielectric constant of the MUT, as captured by (1) derived from the perturbation theory [29]

$$\frac{\Delta f_r}{f_r} = \frac{\int_\Omega (\Delta\varepsilon E_1.E_0 + \Delta\mu H_1.H_0)\, dv}{\int_\Omega \left(\varepsilon_0|E_0|^2 + \mu_0|H_0|^2\right) dv} \tag{1}$$

where Δf_r is the shift in the resonant frequency (f_r) attributable to the MUT. $\Delta\varepsilon$ and $\Delta\mu$ reflect the changes in permittivity and permeability, respectively, induced by the MUT. The variable v represents the differential volume element, with Ω indicating the comprehensive volume of integration that spans the entire area affected by the electromagnetic fields. The fields E_0 and H_0 represent the electric and magnetic distributions before the perturbation, serving as a baseline for understanding the shifts caused by the MUT. E_1 and H_1 are the perturbed field distributions. This equation quantifies the relative change in the resonant frequency of the sensor due to the introduction of the MUT by comparing the perturbed and unperturbed electromagnetic field distributions within the sensing volume.

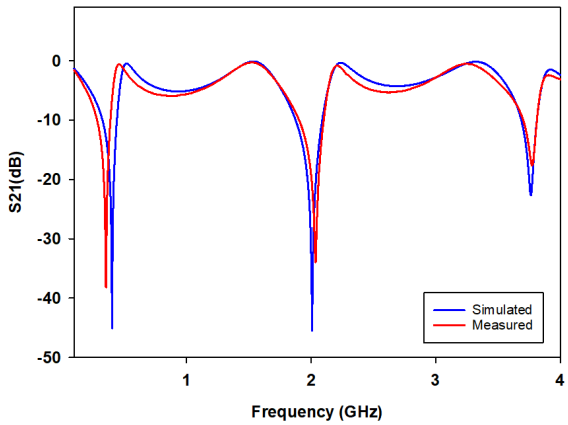

Fig. 2. Comparative analysis of simulated and measured transmission response of the sensor in free space.

In sensing applications, it is essential to optimize the design and specifications of the planar transmission line utilizing defective resonators to increase resonance strength and successfully limit the resonating electrical or magnetic fields inside the sensing area delineated by permittivity or permeability. Indeed, the DH-CSRR structure in the proposed sensor effectively confines the maximum electric field within its slots and edges, enabling enhanced sensitivity to detect even small variations in dielectric properties. Keeping the phosphate sample within the sensing zone leads to an accurate and improved sensitivity.

Fig. 2 presents the simulated and measured transmission response (S_{21}) across the frequency spectrum of the unloaded sensor (free space response). It identifies three distinct resonant frequencies at $f_1 = 0.404$ GHz, $f_2 = 2.007$ GHz, and $f_3 = 3.764$ GHz for the first, second, and third resonances, respectively. While the results generally show good correspondence with the expected response, confirming the sensor's functional validity, some deviations between the simulation and measurement are noted. These discrepancies can be ascribed to factors such as variances in fabrication tolerances, inaccuracies in assembly, and the dielectric properties of the substrate, which can vary with frequency. Furthermore, the soldering of the SMA connectors might also contribute to these discrepancies.

The sensor's wide frequency range, spanning from 0.1 to 4 GHz, is a clear asset in our sensor design. This feature is highly advantageous for material characterization as it provides a wealth of valuable information. The snapshot in Fig. 3 illustrates the magnetic and electric field distribution characteristics of the resonator at its three resonances.

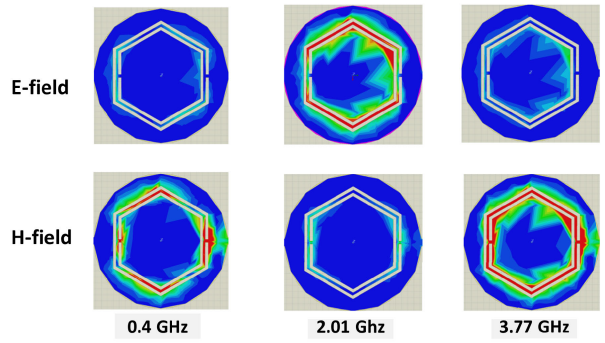

Fig. 3. Comparative magnitude distribution of electric and magnetic fields in a sensor across various frequencies.

The first resonance at 0.4 GHz and the third resonance at 3.77 GHz are characterized by a notable concentration of the magnetic field, contrasting with the second resonance at 2.01 GHz, which shows an increased concentration of the electric field. Furthermore, the third resonance at 3.77 GHz is distinguished by a higher field density, enhancing its sensitivity relative to the first and second resonances.

B. Microwave Properties of Phosphate Powder

The temperature at which the phosphate is exposed significantly influences its quality and attributes. As a result, well-protected and healthy phosphate plays a vital role in industrial quality control, promoting the production of high-quality products and ensuring efficient processes. The application of heat to phosphate can induce various changes, both chemical and physical, which can significantly influence their properties and performance. One notable aspect affected by temperature is the dielectric constant, a property closely related to the chemical changes that occur within the phosphate during heating. It is well known that changes in temperature during the heating process can effectively induce variations in permittivity [30]. Therefore, we investigated the phosphate powder complex permittivity, relying on a coaxial probe as a reliable method to extract the complex dielectric constant [31]. The coaxial probe, which consists of a central conductor, dielectric material, and outer conductor, is a well-established tool widely utilized for assessing the electromagnetic properties of different substances over a large frequency range. In this section, we extend our discussion beyond merely measuring the permittivity of phosphate powder via the coaxial probe method to include the influence of temperature fluctuations on permittivity values.

By analyzing the reflection coefficients (Γ) obtained from the probe, we can determine both the real (ε') and imaginary (ε'') components of the phosphate's complex dielectric constant. This process is facilitated by the instrument's software, employing models such as the Nicholson–Ross–Weir (NRW) method [32]. The complex permittivity of the material is expressed as

$$\varepsilon(\omega) = \varepsilon' - i\varepsilon'' \tag{2}$$

where ε' represents the material's capacity to store electrical energy and $-i\varepsilon''$ accounts for the energy loss within the material.

$$\tan\delta = \frac{\varepsilon''}{\varepsilon'}. \tag{3}$$

Equation (3) describes the material's loss tangent, indicating the ratio of the dissipated energy to the stored energy. This metric is essential for understanding the efficiency of energy storage within the material.

Furthermore, to accurately measure the dielectric properties, we must consider the impedance mismatch between the material and the measurement probe. This mismatch is characterized by the reflection coefficient, Γ, which is defined as

$$\Gamma = \frac{Z_{\text{load}} - Z_0}{Z_{\text{load}} + Z_0} \tag{4}$$

where Z_{load} is the material's impedance and Z_0 is the probe's characteristic impedance. The impedance mismatch is crucial for the software's automatic calculation of ε' and ε''. Utilizing such an approach not only highlights the precision in characterizing dielectric properties but also underscores the importance of considering environmental factors, such as temperature, in our analysis. To ensure accurate measurements of the relative permittivity and dielectric loss factor of the phosphate sample, meticulous sample preparation and a rigorous calibration procedure were crucial. In the following, we provide a detailed description of our methodology.

1. *Sample Preparation:* In our study, we began by preparing a solid disk of phosphate from a 20-mg powder using a Manual Hydraulic Pellet Press, as shown in Fig. 4(a). The disk was meticulously crafted to have a thickness of 3 mm and a radius of 20 mm, ensuring a suitable geometry for the coaxial probe measurements. The main element in the disk was phosphorus (P). To ensure uniformity and consistency, we maintained a consistent weight and applied pressure of 20 MPa during the pellet formation process. This controlled preparation method guarantees reproducibility of the results by minimizing variations in the sample's physical properties.
2. *Calibration Procedure:* To accurately evaluate the relative permittivity and dielectric loss factor of the phosphate sample, we conducted a calibration procedure using known standards with well-defined electrical properties. We employed an open-ended slim probe (Keysight N1501A-102) in conjunction with the PNA-L Network Analyzer N5234B from Keysight Technologies, as shown in Fig. 4(b), to perform reflection coefficient measurements. This setup ensured high precision in the measurements.
3. *Measurement Process:* Careful attention was given to factors such as probe contact, stray capacitance, and parasitic effects during the measurement process. The reflection coefficient (S_{11})was measured over a specified frequency range. Measurements were taken at six different temperatures: 80 °C, 70 °C, 60 °C, 40 °C, 30 °C, and 24 °C. The temperature was controlled using a precision temperature chamber to ensure accurate and consistent conditions.

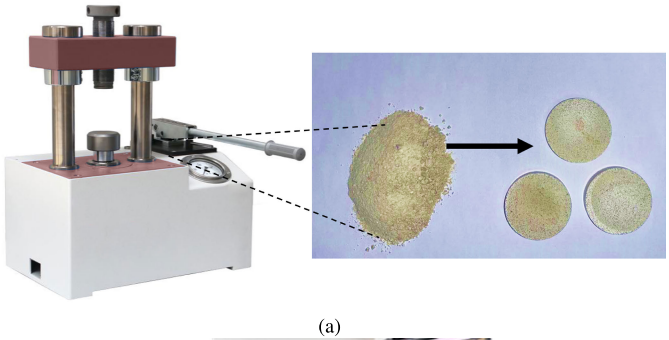

(a)

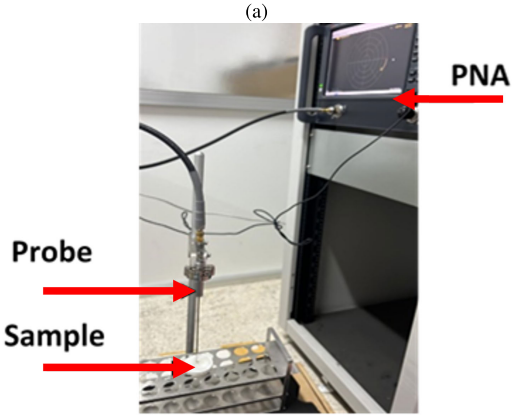

(b)

Fig. 4. (a) Methodology for preparing solid phosphate disks from powder using a manual hydraulic pellet press. (b) Configuration of the coaxial probe measurement setup.

4. *Data Analysis:* The measured S_{11} parameters were analyzed using dielectric measurement software to extract the real and imaginary parts of the permittivity. The software accounted for the calibration standards to ensure the accuracy and reliability of the extracted permittivity values. By following these detailed steps, we ensured accurate and reproducible measurements of the phosphate sample's relative permittivity and dielectric loss factor.

In order to maintain consistent operating conditions and minimize the impact of environmental factors on the collected measurements, the experiments were conducted at a controlled room temperature of 24 °C ± 1 °C. In addition, a holding mechanism was introduced beneath the phosphate sample to ensure repeatability and consistent measurements [see Fig. 4(b)]. The complex permittivity of the phosphate sample was carefully measured at multiple temperatures during the natural cooling process, starting from an initial heating temperature of 80 °C and gradually reaching the ambient room temperature of 24 °C. Achieving this involved recording the complex permittivity values at five different temperatures (70 °C, 60 °C, 40 °C, 30 °C, and 24 °C) throughout the natural cooling process of 1 h, with measurements taken within the frequency range of 0.5–6 GHz. The obtained results are presented in Fig. 5. It is evident from Fig. 5(a) that the real part of the permittivity of the sample before heating demonstrates a consistent behavior throughout the frequency spectrum. The value remains relatively stable, ranging from 4.5 to 4.8. This indicates that the material's ability to store electric potential energy remains stable within the given frequency range,

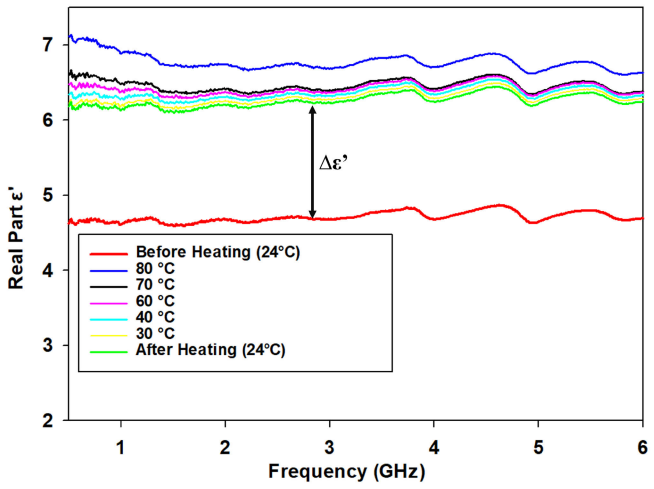

(a)

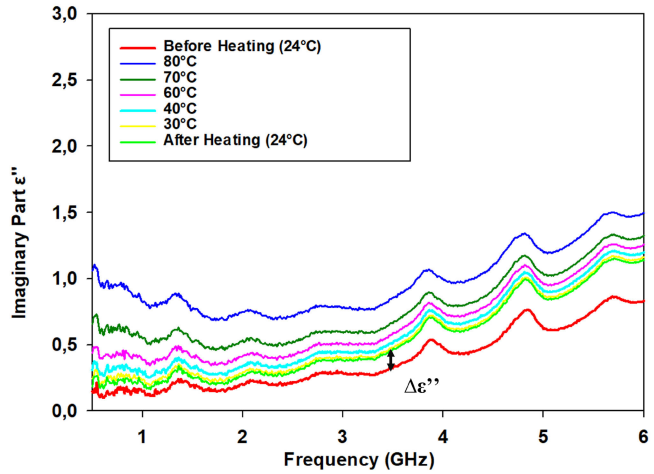

(b)

Fig. 5. (a) Real part. (b) Imaginary part values of phosphate permittivity at various temperatures.

while the imaginary part of the permittivity [see Fig. 5(b)] starts at 0.2 and exhibits an increasing trend as the frequency arises. It reaches a value of 0.8 at the higher end of the frequency range. This behavior suggests that the material exhibits a certain degree of energy dissipation or loss at higher frequencies.

Fig. 5 also illustrates the complex permittivity of the sample at different temperatures between 80 °C and 24 °C. As the temperature gradually decreased, we observed an interesting trend in the permittivity values. At the highest recorded temperature (80 °C), the permittivity value of the phosphate exhibited an increase, reaching 7.2. However, since the sample underwent a natural cooling process for a duration of 1 h, a noteworthy change occurred. When the temperature reached 24 °C, the final permittivity measurement was obtained. The permittivity value exhibited a decrease, ultimately stabilizing within a range of 6.03–6.35 for the real component and 0.21–1.1 for the imaginary component.

These permittivity variations are due to the fact that when the sample is subjected to high temperatures, the motion of the charged particles becomes more chaotic, and the distance between them decreases, resulting in an increase in

the permittivity of the material. This increase in permittivity is due to the increase in thermal energy of the charged particles, causing them to vibrate more and occupy more space, resulting in a stronger dielectric response to an electric field. As the temperature of a sample drops, the movement of its constituent particles slows, causing a decrease in the permittivity of the material. This effect is more pronounced in materials with higher polarizability, such as polar molecules. Even when the phosphate was cooled back down to 24 °C, some residual effects from the previous heating remained. The residual effects kept the relative permittivity elevated at 6.3, even after the temperature returned to its original value. However, it is noteworthy that the difference in complex permittivity between these two situations (before and after heating) remained as $\Delta\varepsilon'$=1.5 for the real part and $\Delta\varepsilon'' = 0.1$ for the imaginary part. This phenomenon is identified as temperature hysteresis, wherein the material retains a memory of its previous thermal conditions. Temperature hysteresis arises because the structural configuration and the alignment and distribution of charged particles within the material do not immediately revert to their initial states upon cooling. This lag in structural response results in a persistent modification of the material's properties, indicating a path-dependent behavior of permittivity [35]. To further explore this behavior, the phosphate permittivity values were input into simulation software to accurately represent phosphate characteristics for each temperature value (80 °C, 70 °C, 60 °C, 40 °C, 30 °C, and 24 °C) across the frequency range from 0.5 to 6 GHz. We will showcase the concurrence between the simulated response of the microwave filter-based sensor, incorporating the Debye model, and the actual measurements obtained when the sensor interacts with the real phosphate sample.

III. Simulation and Experimental Results

The primary aim of this section is to demonstrate the potential of the proposed filter-based sensor in characterizing phosphate, focusing on both simulation and measurement to demonstrate its effectiveness. For this reason, the shift frequency Δf will serve as a parameter to evaluate the sensor's performance under varying temperature conditions, specific to the phosphate. It is defined as the subtraction of the sensor's transmission response frequency at various heating temperatures when a heated phosphate is used, denoted as f_{T_i}, from the reference frequency (f_{ref}), which represents the frequency of the sensor's transmission response when loaded with a phosphate disk measured at room temperature (24 °C), serving as a reference

$$\Delta f = f_{\text{ref}} - f_{T_i} \tag{5}$$

where T_i can take the following temperatures: 80 °C, 70 °C, 60 °C, 40 °C, 30 °C, and 24 °C.

This section is divided into two parts. In Section III-A, we will focus on the simulation of the sensor's performance during the loading process, utilizing the measured dielectric permittivity of the phosphate extracted with the coaxial probe technique under varying temperature conditions. In Section III-B, the sensor will then evaluate the phosphate's dielectric characteristic as it undergoes a cooling process, transitioning from an elevated temperature of 80 °C to the ambient room temperature of 24 °C. The temperature of the solid phosphate was measured by a Medisana TM A7 thermometer. To reduce the impact of environmental factors on the collected measurements and ensure consistent operating conditions for all data, the prepared phosphate disks were tested at a controlled room temperature of 24 °C ± 1 °C.

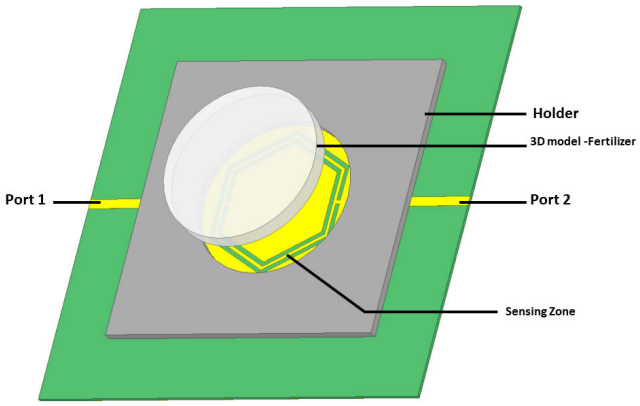

Fig. 6. Simulation setup utilizing the 3-D proposed phosphate model.

A. Simulation and Analysis of the Sensor

To investigate the sensor's capability for tracking the quality of phosphate, the 3-D numerical model shown in Fig. 6, which mimics the proposed microwave sensor, was used to evaluate the complex permittivity of the phosphate placed in the sensing area.

In this model, the phosphate is considered a dielectric material with electrical properties, encompassing both the real and imaginary parts of the complex permittivity values recorded at six distinct temperatures: 80 °C, 70 °C, 60 °C, 40 °C, 30 °C, and 24 °C. The data collected, as presented in Fig. 5, were subsequently used in the 3-D numerical model to perform simulations using a full-wave high-frequency structure simulator (HFSS) over a frequency range of 0.1–4 GHz. A fine mesh with a maximum element size of 0.1 mm was employed to ensure accuracy, with an adaptive mesh refinement process implemented based on S_{21} stability (typically less than a 0.01-dB change in S_{21}). Boundary conditions included a radiation boundary applied to the outer surfaces of the simulation domain, placed at least $\lambda/4$ away from the sensor to emulate open space and minimize reflections. Wave ports were used to excite the structure, with dimensions matching the feeding transmission line to ensure proper impedance matching. The HFSS solver settings were configured for a high-frequency solution type, with a discrete frequency sweep.

The microwave sensor's capability to monitor changes in the phosphate's electrical properties is assessed by recording the transmission coefficient S_{21}. This recording enables the determination of the corresponding frequency shift, denoted as Δf, for each temperature state. For brevity, the S_{21} simulations of the sensor are not presented here.

The obtained simulated results are presented in Table I, which show the frequency shift (Δf) of the three resonances for each temperature value. Table I further illustrates that

TABLE I
HEATING TEMPERATURE VERSUS RESONANCE FREQUENCY SHIFT FOR EACH RESONANCE

Temperature °C	$\Delta_{f_1}(MHz)$	Δ_{f_2}(MHz)	Δ_{f_3}(MHz)
24°C (Before Heating)	0	0	0
80°C	6	42	68
70°C	5	36	60
60°C	4	31	51
40°C	4	27	43
30°C	3,2	21	36
24°C (After Heating)	**2,2**	**16**	**25**

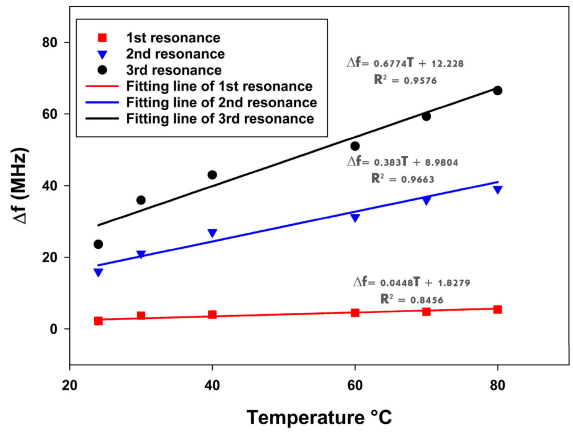

Fig. 7. Simulated results of the resonance frequency shift at different temperatures.

as the temperature of the phosphate progressively decreases, the complex permittivity also decreases (see Fig. 5). Consequently, the sensor's resonances S_{21} gradually shift toward the reference resonant frequency (f_{ref}), resulting in a decrease in Δf.

The observed differences in the frequency shift values at room temperature (24 °C) after heating are approximately 25, 16, and 2.2 MHz for the third, second, and first resonances, respectively. A positive Δf (in this case, 25, 16, and 2.2 MHz) serves as a significant indication of the temperature's impact on the dielectric characteristics of the phosphate. This shift in frequency is also influenced by various factors, including intricate molecular changes and structural adjustments during the cooling process. It reflects the dynamic and nonlinear response of the phosphate, thereby influencing the sensor's resonance behavior. The simulation also demonstrates a higher resonance frequency shift after the natural cooling process at the third resonance, with a value of 25MHz. In addition, the linear analysis conducted on the simulation data reveals a strong linear fit with an R-squared value of $R^2 = 0.9576$ (see Fig. 7).

B. Experimental Results

To validate the simulation results and ensure accuracy in evaluating the sensor's response toward quality change of phosphate for different temperatures, we adopted a thorough experimental method, utilizing the same heating approach as the coaxial probe technique. Our procedure unfolded as follows.

1. Measuring the unloaded sensor's response to establish a baseline, ensuring the sensor is in the calibrated free space response.

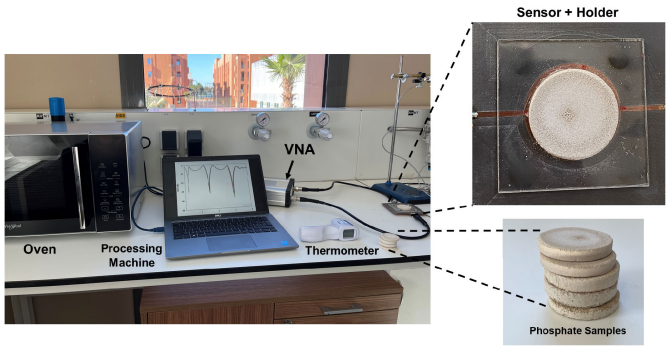

(a)

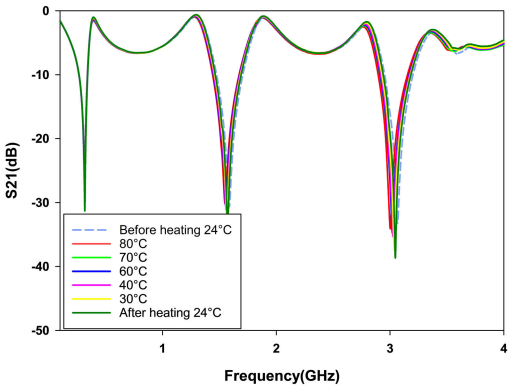

(b)

Fig. 8. (a) Experimental setup for phosphate quality monitoring and testing the performance of the sensor with the VNA. (b) Measured transmission response (S21) at different temperatures for the first, second, and third resonance frequencies before heating, at various temperatures (80 °C, 70 °C, 60 °C, 40 °C, and 30 °C), and after cooling to 24 °C.

2. Measuring the loaded sensor's response with an unaltered phosphate sample before heating, at room temperature (24 °C), to observe its initial interaction in a controlled environment.
3. The solid phosphate sample was heated to 80 °C for 20 min in an oven to ensure uniform thermal conditions.
4. After heating, the natural cooling process began. During this 1-h period, we started our detailed examination by placing the phosphate sample on the sensor and taking a measurement.
5. We repeated the measurement process six times for different temperatures (80 °C, 70 °C, 60 °C, 50 °C, 40 °C, 30 °C, and 24 °C), closely observing the temperature drops.
6. Following the cooling period at 24 °C room temperature, we verified the sensor's response against the baseline to ensure consistency and accuracy in our findings.

This approach maintained consistency and control throughout the experiment. The phosphate sample, with a radius of 20 mm and a thickness of 3 mm, remained positioned on the prototype sensor throughout the cooling process. Notably, the measurements were conducted in real time during the cooling process to emulate online monitoring of the phosphate. Fig. 8(a) illustrates the prototype sensor's design tailored specifically for analyzing the solid phosphate's dielectric properties across a range of temperatures, including 80 °C, 70 °C,

60 °C, 40 °C, 30 °C, and 24 °C. In order to evaluate the effect of temperature on the phosphate, the prepared solid sample is loaded within the sensing zone of the sensor, which generates a high-intensity electromagnetic field. Subsequently, the results obtained at various temperatures were compared to the reference response of an unaltered solid phosphate (referred to as "Before Heating at 24 °C"). The reference response, denoted as f_{ref}, serves as a reference response for comparison.

In order to accurately measure the shift frequency, S_{21}-parameter measurements are taken using the pico-vector network analyzer (VNA) 108. This device offers a high-frequency resolution of 0.03 MHz and a magnitude resolution of 0.01 dB. The Short, Open, Load, Through (SOLT) kit is employed to perform VNA calibration within the frequency range of 0.1–4 GHz, with a frequency increment of 0.01 MHz. These types of VNA are utilized for laboratory measurement due to their high precision and capability. However, for in situ measurements, the flexibility of using a handheld VNA such as the Nano VNA instead of a traditional laboratory-based VNA enhances the sensor's applicability in field assessments. This allows for more versatile and convenient testing scenarios. Fig. 8(b) shows the measured transmission coefficient response of the proposed prototype. In this measurement, we first recorded the transmission response of the sensor for the reference sample of the phosphate (before heating at 24 °C). The main resonance frequencies before heating are $f_{\text{ref1}} = 0.3168$ GHz, $f_{\text{ref2}} = 1.5859$ GHz, and $f_{\text{ref3}} = 3.0675$ GHz. These recorded reference frequencies will be used to assess any frequency changes that occur when the phosphate sample is subjected to varying temperature levels.

The Medisana TM A7 thermometer was used to measure the temperature of the phosphate. The measured transmission frequency response of the sensor for each temperature is presented in Fig. 8(b), and the details on the variation of the S_{21} response at the three resonances are depicted in Fig. 9. By tracking the decrease in temperature of the phosphate, high sensitivity was observed while the resonance frequencies shifted back toward higher frequencies. This persistent deviation indicates that the effects of the heating process endure even after the temperature has been reduced. During the cooling-down phase, although the phosphate temperature decreases to room temperature, the physical changes induced by heating, such as molecular rearrangements and bond formations, did not completely reverse. As a result, the altered characteristics of the phosphate persist, impacting the resonance frequencies. These frequencies, influenced by the effective permittivity and other material properties, did not return to their original reference values due to the lingering effects of the heating process. After heating the sample of phosphate and allowing it to cool down for 1 h, it was observed that the resonance frequencies did not revert back to the reference frequency values.

Our findings reveal that for each resonance frequency, the frequency shift increases as the temperature rises, as depicted in Fig. 10. After the normal cooling process of 1 h to reach room temperature (24 °C), distinct frequency shifts were observed for the three resonances. The third resonance

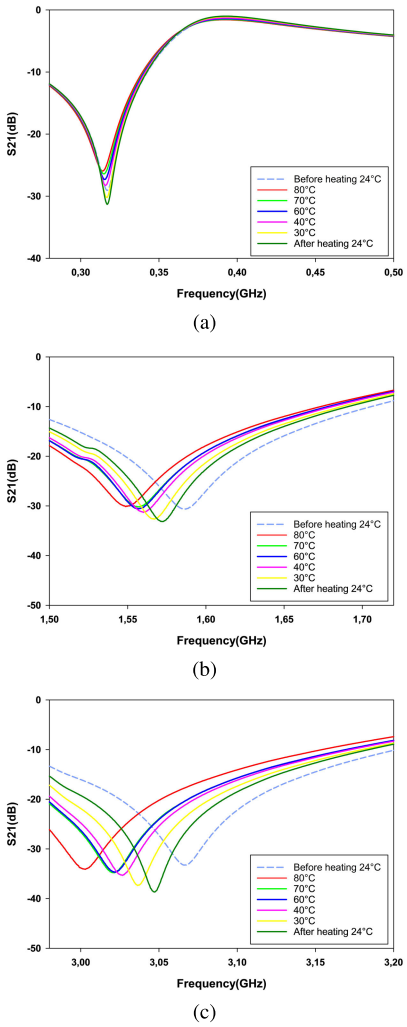

Fig. 9. Detailed of (a) first, (b) second, and (c) third resonances measured transmission response at different temperatures.

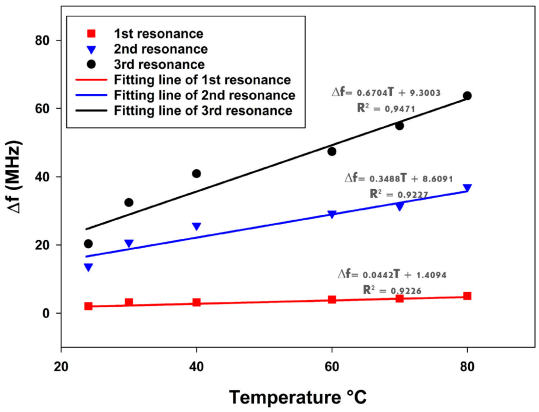

Fig. 10. Measured results of the resonance frequency shift at different temperatures for the three resonances.

displayed a higher frequency shift of 20.3 MHz, while the second and first resonances exhibited lower shifts of 13.7 and 1 MHz, respectively. This difference in the frequency shift for the three resonances can be explained using the results presented in Fig. 3, along with consideration of the wavelength for each resonance frequency. Higher

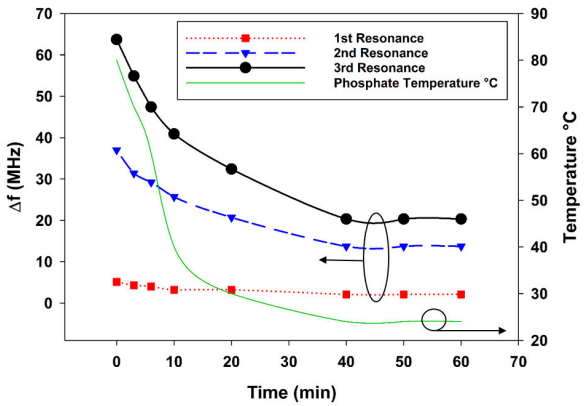

Fig. 11. Time-domain results of the resonance frequency shift for the three resonances.

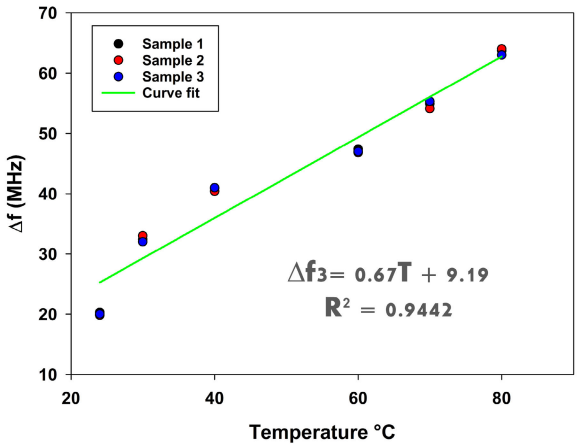

Fig. 12. Repeatability verification of third resonance frequency shifts ($\Delta f3$) at various temperatures for different phosphate samples.

frequency resonances correspond to shorter wavelengths, enabling more precise spatial resolution and stronger interactions with the phosphate. Consequently, the third resonance, having the highest frequency and the shortest wavelength, experiences more pronounced interactions and greater sensitivity to temperature-induced changes in the phosphate's effective permittivity. As a result, it exhibits a larger frequency shift compared to the second and first resonances, which have longer wavelengths and correspondingly less pronounced interactions with the phosphate. The resonance frequency shifts toward the three different resonances and temperatures were analyzed using linear regression. The obtained results depicted in Fig. 10 demonstrate a strong correlation with a linear fit of $R^2 = 0.9471$ for the third resonance. In this study, we aim to observe the effect of heating on the characteristics of phosphate samples. The sensing mechanism focuses on comparing the frequency shifts of the sensor when the heated phosphate is cooled down to room temperature (24 °C) with a reference phosphate sample that is already at 24 °C. This approach ensures that our analysis captures frequency shifts due to permanent changes in the phosphate's properties induced by temperature, rather than transient effects during heating and cooling. By doing so, we avoid the impact of temperature hysteresis on the sensor readings.

Fig. 11 illustrates the real-time frequency shift (Δf) of the sensor over the cooling period of 60 min, demonstrating its dynamic response to temperature variations. The graph shows the behavior of the first, second, and third resonance frequencies alongside the temperature changes. The first resonance exhibits a minimal frequency shift, stabilizing at approximately 2 MHz throughout the period. The second resonance shows a moderate frequency shift, decreasing from around 38–16 MHz. The third resonance displays the most substantial frequency shift, decreasing from approximately 65 to 25 MHz. Notably, the frequency shifts for all three resonances stabilize starting from the 40-min mark. It was found that the change in the frequency shift exhibits the same trend as the temperature changes, indicating that the microwave sensor is suitable for real-time quality sensing of the phosphate within the temperature range of 24 °C–80 °C.

Moreover, to evaluate the sensor's reproducibility, we conducted measurements from three different phosphate samples, each heated to 80 °C over 20 min and then placed in the sensitive region of the sensor. For each sample, the frequency shift, especially for the third resonance, was carefully calculated during the subsequent cooling process over 1 h. The obtained results are depicted in Fig. 12. The data represented by black dots for sample 1, red dots for sample 2, and blue dots for sample 3 exhibit high consistency, with closely clustered groups at each temperature point, indicating high repeatability. The linear fit, $\Delta f3 = 0.67\ T + 9.19$, shows a predictable relationship where Δf increases by 0.67 MHz/°C, starting from 9.19 MHz. This relationship is validated by an R-squared value of 0.9442, meaning that 94.42% of the variability in Δf is explained by temperature changes. The strong alignment of data points with the model highlights the sensor's potential for accurate temperature monitoring in scientific and industrial applications.

Achieving the highest accuracy in our measurements and effectively managing potential temperature crosstalk between the sensor and the sample during frequency shift detection requires a thorough understanding of the calibration dynamics of the sensor, especially when it is loaded with a heated sample. Temperature crosstalk can significantly distort the measurement accuracy, thereby affecting the reliability of real-time monitoring applications.

To address this, it is recommended to perform a comprehensive calibration procedure that focuses on calculating the relative error attributable to the sensor itself, after exposure to a temperature of 80 °C. This approach helps in clarifying the thermal transfer phenomena that may occur from the heated phosphate sample to the sensor, thereby facilitating the identification and reduction of temperature crosstalk. This calibration strategy is crucial for enhancing the precision of our measurements, ensuring that the shift frequency reflects sample changes rather than measurement artifacts.

The detailed calibration procedure includes the following steps.

1. *Initial Baseline Measurement:* Begin by recording the sensor's transmission frequency response in free space at ambient room temperature (24 °C) to establish a baseline frequency for each resonance.

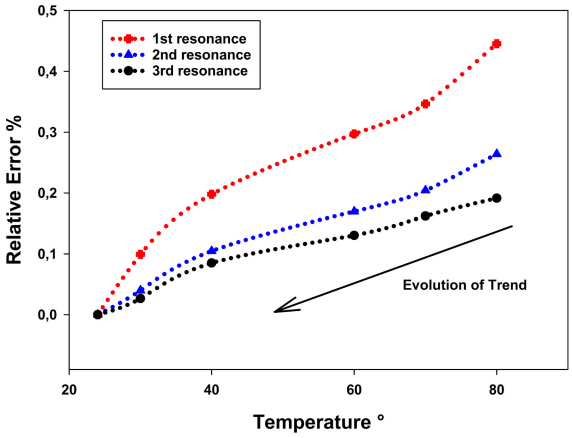

Fig. 13. Relative errors in the resonance frequency shift for the sensor in free space for the three resonances.

2. *Heating Phase:* Heat the phosphate sample to 80 °C, and allow it to calibrate. Place the heated sample in close proximity to the sensor, and record the new transmission frequency response.
3. *Cooling Phase:* After the measurement with the heated sample, allow the sensor to cool down to room temperature (24 °C) over a period of 1 h. Record the transmission frequency response at intervals during the cooling phase to monitor changes.
4. *Relative Error Calculation:* Calculate the relative error using the formula

$$\text{Relative Error } \% = \frac{f_{\text{heated}} - f_i}{f_i} \times 100 \tag{6}$$

where f_{heated} represents the sensor's transmission frequency response at various temperatures and f_i denotes the initial frequency of the sensor's resonance (with i representing the resonance order: 1, 2, or 3).
5. *Data Analysis and Adjustment:* Analyze the relative error data to identify any systematic errors or deviations. Use this analysis to adjust the sensor readings, thereby compensating for any temperature-induced variations.
6. *Verification and Repeatability Testing:* Repeat the calibration procedure with multiple samples to verify the consistency and repeatability of the sensor's performance under thermal stress.

As can be seen from Fig. 13, the relative error of the sensor displays a downward trend, indicating a decrease in error as the sensor cools from an initially heated state of 80 °C. For the first resonance, the sensor error percentage begins close to 0.5% at the highest temperature and decreases to 0% as the sensor returns to the ambient baseline temperature of 24 °C. The second and third resonances exhibit a similar pattern of reduction, starting with error percentages around 0.25% and 0.15% at 80 °C, respectively, which then declines as the temperature decreases. This reduction in relative error to 0% for all three resonances demonstrates that at 24 °C, the sensor exhibits no thermal influence on its frequency response, indicating its thermal stability under operational conditions. This downward trend is likely due to the temperature-dependent variations in the dielectric properties of the substrate within the sensor, which affects the electromagnetic behavior and, consequently, the resonance characteristics. The slight relative errors observed in the sensor's frequency response, due to thermal effects, are minimal and within acceptable limits for accurate real-time temperature monitoring. These errors, effectively managed through calibration, do not affect the sensor's ability to deliver precise temperature readings of samples.

IV. Discussion

In this article, we propose a proof of concept for a novel approach utilizing a filter-based sensor, which aims to elucidate the impact of temperature on the dielectric properties of phosphate, thereby assessing its quality through the analysis of microwave signals. We introduce a specialized filter-based sensor, meticulously designed for the accurate monitoring of phosphate quality under a spectrum of temperature conditions. This sensor finds its critical application in scenarios such as the storage and transportation of phosphate in tropical environments, where the risk of spoilage is paramount. The essence of our methodology lies in understanding the interactions between electromagnetic waves and materials, with a particular emphasis on detecting shifts in dielectric properties induced by temperature changes. These shifts are invaluable in assessing the material's behavior and serve as essential indicators of quality alterations in the phosphate at different temperatures. Furthermore, calibrating for temperature crosstalk is vital for real-time measurement accuracy. Our strategy involved offline measurements to establish a baseline sensor response across a known temperature range. This approach showed minimal sensor errors, affirming data accuracy and reliability for sample quality assessment. After establishing this assurance, our subsequent analysis focuses on the resonance shift frequency data presented in Fig. 7 (simulated values) and Fig. 10 (measured values). We employ the root mean square error (RMSE) as a crucial metric to quantify the discrepancies between these two datasets

$$\text{RMSE} = \sqrt{\frac{1}{4} * \sum_{i=1}^{k} \left(\Delta_{f\,i} - \Delta_f\right)}. \tag{7}$$

The RMSE provides a succinct measure of the average differences between the predicted and observed resonance shift frequencies, offering a quantitative evaluation of our sensor model's accuracy. A lower RMSE suggests a closer agreement between the simulated values and the measured values, emphasizing the reliability of our predictive model. The RMSE values, computed to compare simulated and measured resonance shift frequencies for the first, second, and third resonances, are specifically 0.44, 2.2, and 3.28, respectively.

V. Conclusion

In conclusion, the study introduces a microwave sensor with a double-hexagonal CSSR (DH-CSSR) for real-time monitoring of phosphate quality while investigating the temperature impact. To the best of the authors' knowledge, this study represents the first instance of investigating phosphate quality in this manner. The microwave sensor is designed primarily

to track how the dielectric properties of the phosphate are influenced by changed temperature based on measuring the frequency shift (Δf). The measurements were conducted for the three resonances of the microwave sensor, showcasing the sensor's notable reliability, particularly for the third resonance, which exhibited high sensitivity with a frequency shift of 20 MHz after being heated to 80 °C. The primary function of the proposed microwave sensor is to determine whether the phosphate has been subjected to elevated temperatures during storage and transportation, providing insight into its quality. In addition, the study analyzed the relative error of the sensor to avoid crosstalk and ensure that our results are attributed mainly to the change in characteristics of the phosphate. The results show a minimal relative error, concluding that the effect is negligible. We also evaluated the RMSE between the simulated value of Δf for the proposed model extracted from the coaxial probe technique and the measured values. It shows a low RMSE of about 0.44, 2.2, and 3.28, respectively, for the first, second, and third resonance shift frequencies. The proposed microwave sensor presents a compelling set of advantages, including its compact size for unobtrusive integration, high sensitivity enabling precise detection, a streamlined manufacturing process with no fabrication complexities, and consistent performance for reliable data output across various conditions. These features collectively make the sensor a versatile, reliable, and cost-effective solution in sensing technology.

REFERENCES

[1] H. Z. Toama, "World phosphate industry," *Iraqi Bull. Geol. Mining*, vol. 7, pp. 5–23, 2017.

[2] A. O. Fayiga and O. C. Nwoke, "Phosphate rock: Origin, importance, environmental impacts, and future roles," *Environ. Rev.*, vol. 24, no. 4, pp. 403–415, Dec. 2016, doi: 10.1139/er-2016-0003.

[3] M. A. de Boer, L. Wolzak, and J. C. Slootweg, "Phosphorus: Reserves, production, and applications," in *Phosphorus Recovery and Recycling*, H. Ohtake and S. Tsuneda, Eds., Singapore: Springer, 2019, doi: 10.1007/978-981-10-8031-9_5.

[4] L. Hermann, F. Kraus, and R. Hermann, "Phosphorus processing—Potentials for higher efficiency," *Sustainability*, vol. 10, no. 5, p. 1482, May 2018, doi: 10.3390/su10051482.

[5] D. D'Huile, "Caractérisation et impacts environnementaux," *Environ. Technol.*, vol. 26, pp. 35–45, Dec. 2005.

[6] K. Najim, M. Najim, and H. Youlal, "Self-tuning control of an industrial phosphate dry process," *Optim. Control Appl. Methods*, vol. 3, no. 4, pp. 435–442, Oct. 1982.

[7] C. C. Corredor, D. Bu, and D. Both, "Comparison of near infrared and microwave resonance sensors for at-line moisture determination in powders and tablets," *Anal. Chim. Acta*, vol. 696, nos. 1–2, pp. 84–93, Jun. 2011, doi: 10.1016/j.aca.2011.03.048.

[8] S. S. Goyal, "Use of high performance liquid chromatography for soil and plant analysis," *Commun. Soil Sci. Plant Anal.*, vol. 33, nos. 15–18, pp. 2617–2641, Nov. 2002, doi: 10.1081/css-120014468.

[9] G. E. Acquah et al., "Portable X-ray fluorescence (pXRF) calibration for analysis of nutrient concentrations and trace element contaminants in fertilisers," *PLoS ONE*, vol. 17, no. 1, Jan. 2022, Art. no. e0262460, doi: 10.1371/journal.pone.0262460.

[10] C. Zhu and J. Huang, "Coaxial cable sensing: Review and perspective," *IEEE Trans. Microw. Theory Techn.*, vol. 72, no. 3, pp. 1790–1809, Mar. 2024.

[11] J. Muñoz-Enano, P. Vélez, M. Gil, and F. Martín, "Planar microwave resonant sensors: A review and recent developments," *Appl. Sci.*, vol. 10, no. 7, p. 2615, Apr. 2020, doi: 10.3390/app10072615.

[12] M. M. Bait-Suwailam, R. M. Tbaileh, H. Al-Lawati, and Y. Al-Mulla, "Perspective chapter: Microwave sensors for soil moisture detection—An application toward healthy date palm," in *New Insights in Soil-Water Relationship*. IntechOpen, Jul. 2024, doi: 10.5772/intechopen.109152.

[13] M. Vreugdenhil et al., "Microwave remote sensing for agricultural drought monitoring: Recent developments and challenges," *Frontiers Water*, vol. 4, p. 205, Nov. 2022, doi: 10.3389/frwa.2022.1045451.

[14] S. Trabelsi and S. O. Nelson, "Microwave sensing of quality attributes of agricultural and food products," *IEEE Instrum. Meas. Mag.*, vol. 19, no. 1, pp. 36–41, Feb. 2016, doi: 10.1109/MIM.2016.7384959.

[15] V. Yadav, A. Kumar, S. Sharan, and A. K. Sinha, "Analyses of dielectric properties of fertilizers (urea and diammonium phosphate) in aqueous solution at different temperatures in microwave frequency," *Int. J. Phys. Sci.*, vol. 5, no. 16, pp. 2466–2470, 2010.

[16] Y. Zaarour et al., "The quality monitoring of paracetamol medicament using a noninvasive microwave sensor," *Sci. Rep.*, vol. 13, no. 1, p. 17443, Oct. 2023, doi: 10.1038/s41598-023-43409-y.

[17] M. E. Gharbi, M. Martinez-Estrada, R. Fernández-García, and I. Gil, "Determination of salinity and sugar concentration by means of a circular-ring monopole textile antenna-based sensor," *IEEE Sensors J.*, vol. 21, no. 21, pp. 23751–23760, Nov. 2021, doi: 10.1109/JSEN.2021.3112777.

[18] V. Turgul and I. Kale, "Permittivity extraction of glucose solutions through artificial neural networks and non-invasive microwave glucose sensing," *Sens. Actuators A, Phys.*, vol. 277, pp. 65–72, Jul. 2018, doi: 10.1016/j.sna.2018.03.041.

[19] S. Harnsoongnoen, A. Wanthong, U. Charoen-In, and A. Siritaratiwat, "Planar microwave sensor for detection and discrimination of aqueous organic and inorganic solutions," *Sens. Actuators B, Chem.*, vol. 271, pp. 300–305, Oct. 2018, doi: 10.1016/J.SNB.2018.05.077.

[20] S. Yee et al., "Microwave sensing of ammonia and iron concentration in water based on complementary double split-ring resonator," *Sens. Actuators Rep.*, vol. 3, Nov. 2021, Art. no. 100044, doi: 10.1016/j.snr.2021.100044.

[21] F. Deshours et al., "Improved microwave biosensor for non-invasive dielectric characterization of biological tissues," *Microelectron. J.*, vol. 88, pp. 137–144, Jun. 2019.

[22] J.-K. Park, T.-G. Kang, B.-H. Kim, H.-J. Lee, H. H. Choi, and J.-G. Yook, "Real-time humidity sensor based on microwave resonator coupled with PEDOT:PSS conducting polymer film," *Sci. Rep.*, vol. 8, no. 1, Jan. 2018, Art. no. 439.

[23] J. Huang and Y. Xiang, "Injection-locked-oscillation-based active sensor on dual-mode folded SIW rectangular cavity for high-resolution detection to moisture and Fe particle in lubricant oil," *IEEE Trans. Microw. Theory Techn.*, vol. 71, no. 4, pp. 1600–1611, Apr. 2023.

[24] H. Mirzaei, J. McClelland, D. Sharma, M. Arjmand, and M. H. Zarifi, "A microwave voyage into swelling phenomenon: Investigation of polydimethylsiloxane and VOCs interaction," *ACS Appl. Mater. Interfaces*, vol. 15, no. 31, pp. 38008–38017, Aug. 2023.

[25] S. Harnsoongnoen, A. Wanthong, U. Charoen-In, and A. Siritaratiwat, "Microwave sensor for nitrate and phosphate concentration sensing," *IEEE Sensors J.*, vol. 19, no. 8, pp. 2950–2955, Apr. 2019, doi: 10.1109/JSEN.2018.2890462.

[26] S. Harnsoongnoen, "Metamaterial-inspired microwave sensor for detecting the concentration of mixed phosphate and nitrate in water," *IEEE Trans. Instrum. Meas.*, vol. 70, pp. 1–6, 2021, doi: 10.1109/TIM.2021.3086901.

[27] R. Marqués, F. Martin, and M. Sorolla, *Metamaterials With Negative Parameters: Theory, Design, and Microwave Applications*. Hoboken, NJ, USA: Wiley, 2011.

[28] H.-Y. Gan et al., "A CSRR-loaded planar sensor for simultaneously measuring permittivity and permeability," *IEEE Microw. Wireless Compon. Lett.*, vol. 30, no. 2, pp. 219–221, Feb. 2020.

[29] D. M. Pozar, *Microwave Engineering*. Hoboken, NJ, USA: Wiley, 2011.

[30] M. Lazebnik, M. C. Converse, J. H. Booske, and S. C. Hagness, "Ultrawideband temperature-dependent dielectric properties of animal liver tissue in the microwave frequency range," *Phys. Med. Biol.*, vol. 51, no. 7, pp. 1941–1955, Apr. 2006.

[31] M. El Khamlichi, A. Alvarez Melcon, O. El Mrabet, M. A. Ennasar, and J. Hinojosa, "Flexible UHF RFID tag for blood tubes monitoring," *Sensors*, vol. 19, no. 22, p. 4903, Nov. 2019.

[32] A. M. Nicolson and G. F. Ross, "Measurement of the intrinsic properties of materials by time-domain techniques," *IEEE Trans. Instrum. Meas.*, vol. IM-19, no. 4, pp. 377–382, Nov. 1970, doi: 10.1109/TIM.1970.4313932.

[33] H. Zhang, R. P. Voroney, and G. W. Price, "Effects of temperature and activation on biochar chemical properties and their impact on ammonium, nitrate, and phosphate sorption," *J. Environ. Qual.*, vol. 46, no. 4, pp. 889–896, Jul. 2017.

[34] D. Meisak et al., "Effect of temperature on shielding efficiency of phosphate-bonded $CoFe_2O_{4-x}BaTiO_3$ multiferroic composite ceramics in microwaves," *J. Mater. Res. Technol.*, vol. 24, pp. 1939–1948, May 2023.

[35] T. W. Dakin, "Conduction and polarization mechanisms and trends in dielectric," *IEEE Elect. Insul. Mag.*, vol. 22, no. 5, pp. 11–28, Sep. 2006, doi: 10.1109/mei.2006.1705854.

Youness Zaarour (Student Member, IEEE) received the bachelor's degree in electronics from Cadi Ayyad University, Marrakesh, Morocco, in 2018, and the M.Sc. degree in electronics and telecommunication from Abdelmalek Essaadi University, Tetouan, Morocco, in 2020. He is currently pursuing the Ph.D. degree with the Microwave Sensing and Energy (MSE) Department, University Mohammed VI Polytechnic (UM6P), Ben Guerir, Morocco.

In 2020, he held a position as a Research Assistant at the Information and Telecommunication Systems Laboratory (LaSIT) Department, Faculty of Sciences, Tetouan. He is currently working on monitoring biological microwave sensors. He has actively participated in numerous conferences and has been recognized for his exceptional contributions, receiving four gold medals in different categories, including medical and agricultural applications.

Mr. Zaarour was awarded the Erasmus + Mobility Grant.

Fatima Zahrae El Arroud (Student Member, IEEE) received the bachelor's degree in electronics and the M.Sc. degree in telecommunication systems engineering from Abdelmalek Essaâdi University, Tetouan, Morocco, in 2018 and 2020, respectively. She is currently pursuing the Ph.D. degree with the Department of Microwave Energy Sensing (MES), Digital Innovation Center of Excellence (DICE), University of Mohammed VI Polytechnic, Ben Guerir, Morocco.

In 2020, she held a position as a Research Assistant at the Information and Telecommunication Systems Laboratory (LaSIT), Faculty of Sciences, Tetouan.

Otman El Mrabet (Member, IEEE) received the M.Sc. and Ph.D. degrees from the University of Abdelmalek Essaadi, Tetouan, Morocco, in 2000 and 2004, respectively.

From March to October 2005, he was a Visiting Researcher with the Rennes Institute of Electronics and Telecommunications, Rennes, France. From 2007 to 2009, he was a Post-Doctoral Researcher with the Electrical and Electronic Engineering Department, UPNA, Pamplona, Spain, under the AECI Fellowship. Since 2009, he has been an Assistant Professor with the LaSiT Laboratory, Abu Dhabi, UAE, where he supervises several Ph.D. and M.Sc. theses. He is a Fulbright Scholar with the University of Wisconsin Madison, Madison, WI, USA, in 2019. His research interests include UWB antenna design, metamaterials and metasurfaces, RFID tag antennas, rectennas and wireless power transfer, and modeling active circuits using the finite-difference time-domain method (FDTD).

Abdessamad Faik received the Ph.D. degree from the University of the Basque Country, Leioa, Spain, in 2009.

After his Ph.D., he obtained a Postdoctoral Fellowship with CEMTHI Laboratory, CNRS, Orleans, France. He then worked as a Guest Scientist with German Aerospace Center (DLR), Stuttgart, Germany. Finally, he joined CIC EnergiGUNE, Vitoria-Gasteiz, Spain, as a Team Leader of the materials development and corrosion study, coordinating the activities of the researchers within the research projects. He is currently the Director of LIMSET, Laboratory of Inorganic Materials for Sustainable Energy Technologies, Ben Guerir, Morocco. He has published more than 107 peer-reviewed articles and six international patents and presented more than 100 contributions to international conferences.

Rafiq El Alami received the Engineering degree from Ecole Mohammadia d'Ingénieurs, Rabat, Morocco, in 1996, and the M.B.A. degree from UM6P/Columbia University, New York, NY, USA, in 2019.

He is the Director of the Digital Innovation Center of Excellence (DICE), Ben Guerir, Morocco, DICE is a center that collaborates with all UM6P's departments to apply digital technologies (big data, AI, crowdsourcing, and mobility) to accelerate research and innovation. Before he joined UM6P, has spent 18 years in different management positions with Microsoft, Redmond, WA, USA.

Hafid Griguer (Member, IEEE) received the master's degree from the University of Metz, Metz, France, in 2005, and the Ph.D. degree in microelectronics from the National Institute of Applied Sciences, Rennes, France, in 2010.

He is a Vice Director of the Digital Innovation Center of Excellence (DICE), Mohammed VI Polytechnic University (UM6P), Ben Guerir, Morocco. His work spans digital industrialization, developing innovative sensor and microwave antenna concepts for industrial and medical use. An inventor holding multiple patents, he has authored numerous articles and book chapters.

Dr. Griguer is a member of the IEEE, contributing significantly to the field of electronic systems engineering.